J|A|C|S

A R T I C L E S

Building Up Key Segments of *N*-Glycans in the Gas Phase: Intrinsic Structural Preferences of the α(1,3) and α(1,6) Dimannosides

Pierre Çarçabal,[†] Isabel Hünig,[†] David P. Gamblin,[‡] Bo Liu,[†]
Rebecca A. Jockusch,[†,‡] Romano T. Kroemer,[§] Lavina C. Snoek,[†]
Anthony J. Fairbanks,[‡] Benjamin G. Davis,[‡] and John P. Simons*,[†]

*Contribution from the Physical and Theoretical Chemistry Laboratory, University of Oxford,
South Parks Road, OX13QZ Oxford, United Kingdom, Sanofi-Aventis, Centre de Recherche de
Paris, 13 quai Jules Guesde, BP14, 94403 Vitry-sur-Seine, France, and Chemistry Department,
Chemistry Research Laboratory, 12 Mansfield Road, Oxford OX1 3TA United Kingdom*

Abstract: The intrinsic conformer specific vibrational spectra of two important subunits of the core pentasaccharide of N-linked glycans, the α(1,3) and α(1,6) dimannosides, have been recorded in the gas phase. Coupling these measurements with a computational exploration of their conformational landscapes has enabled their conformational assignment and has identified characteristic vibrational signatures associated with particular conformational families—including those that do or do not display inter-ring hydrogen bonding across the glycosidic linkage. In addition, the IR spectra of the monosaccharide moieties provide benchmarks, through which the conformational assignments can be refined. This introduces a general concept of modularity and secondary structure in oligosaccharides—essential for the success of similar studies on larger oligosaccharides in the future.

Introduction

It is now well-established that the co- and posttranslational glycosylation of proteins is fundamental to a variety of biological processes to include immunity,[1] fertilization,[2] and protein stability.[3] The extensive role of carbohydrates in nature may be explained by the density of structural information portrayed by glycans due to their extensive permutations of oligosaccharide structures.[4] However, in fact, nature relies upon only a select few motifs from its potentially extensive library. In particular, the carbohydrate motifs of *N*-glycans are well-conserved around the central pentasaccharide core $Man_3GlcNAc_2$ and are often critical to the future prospects of the glycoprotein. Moreover, the carbohydrate motif, the so-called glycocode, found on maturing glycoproteins is indicative of the proteins' age, structure, and localization.[5] This information can be interpreted by a variety of lectins, transferases, and glycosidases that assist in the construction and trafficking of both native and defective glycoproteins within the cell. For example, nascent glycoproteins emerge from the ribosome and interact with the molecular chaperones calnexin and calreticulin, via their terminal glucose

residue of $Glc_1Man_9GlcNAc_2Asn$.[5] This process promotes correct protein folding, resulting in the eventual release of native proteins into the secretory pathway. Misfolded glycoproteins reenter the calnexin/calreticulin cycle through repeated glucosylation−deglucosylation following the actions of glucosidase II and UDP-Glc/glycoprotein glucosyltransferase.[6] Persistently misfolded proteins are eventually trimmed of their terminal mannose by the action of α-mannosidase I, causing the incompetent protein to enter the endoplasmic reticulum-associated protein degration (ERAD) pathway via the critical recognition by mannose binding lectins EDEM and EDEM2 of the recurrent structural motifs of the D1, D2, and D3 arms of processed *N*-glycans (Figure 1).[7] Although these glycobiological motifs have long been identified and studied,[8] the underlying reasons for their selection by nature as motifs for such critical recognition remains to be understood. A bottom-up strategy that first identifies their intrinsic structural properties in the gas phase and then explores the response of these properties to different environments[9] provides an important de novo path towards this understanding.

In a first step along this path, we have investigated the gas phase conformational choices of the α(1,6) and α(1,3) linked dimannosides, the two nonreducing terminal arms of the

[†] University of Oxford.
[‡] Chemistry Research Laboratory.
[§] Centre de Recherche de Paris.

(1) Lowe, J. B. *Cell* **2001**, *104*, 809−812.
(2) Talbot, P.; Shur, B. D.; Myles, D. G. *Biol. Reprod.* **2003**, *68*, 1−9.
(3) Rudd, P. M.; Joao, H. C.; Coghill, E.; Fiten, P.; Saunders: M. R.; Opdenakker, G.; Dwek, R. A. *Biochemistry* **1994**, *33*, 17−22. Parodi, A. J.; *Annu. Rev. Biochem.* **2000**, *69*, 69−93.
(4) Davis, B. G. *Chem. Rev.* **2002**, *102*, 579−602. Laine, R. A.; *Glycobiology* **1994**, *4*, 759−767.
(5) Helenius, A.; Abei, M. *Science* **2001**, *291*, 2364−2369.
(6) Hammond, C.; Braakman, I.; Helenius, A. *Proc. Natl. Acad. Sci. U.S.A.* **1994**, *91*, 913−917.
(7) Hebert, D. N.; Garman, S. C.; Molinari, M. *Trends Cell Biol.* **2005**, *15*, 364−370. Spiro, R. G. *Cell Mol. Life Sci.* **2004**, *61*, 1025−1041.
(8) Wormald, M. R.; Petrescu, A. J.; Pao, Y. L.; Glithero, A.; Elliott, T.; Dwek, R. A. *Chem. Rev.* **2002**, *102* (2), 371−386 and references therein.
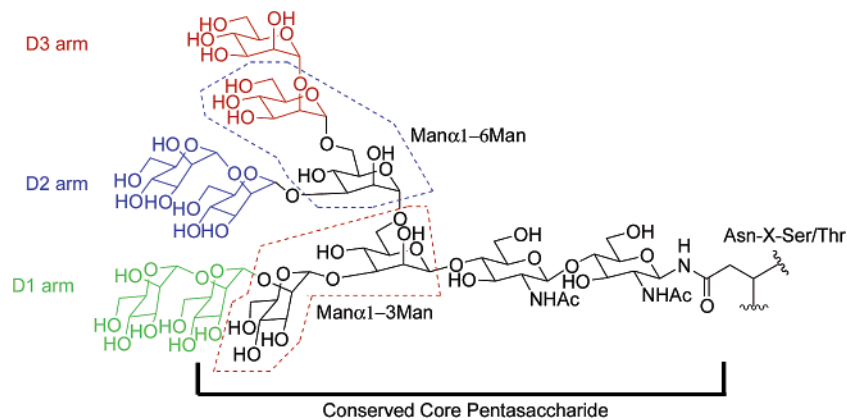(9) Kirschner, K. N.; Woods, R. J. *Proc. Natl. Acad. Sci. U.S.A.* **2001**, *98*, 10541−10545.

Figure 1. Recurrent *N*-glycan motif of glycoproteins including the D1, D2, and D3 arms as well as the *N*-Asn linkage.
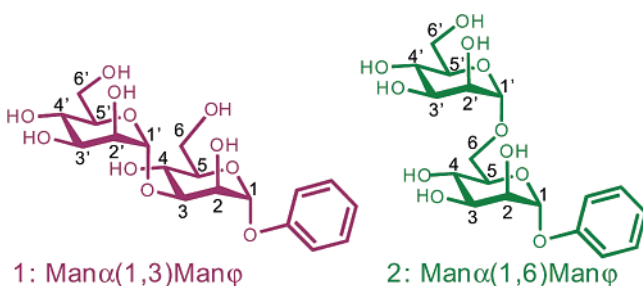

Figure 2. Structural formulas of dimannosides **1** and **2** under investigation. The numbering of the carbons and of the corresponding OH groups is illustrated.

pentasaccharide and key starting motifs of the D1, D2, and D3 arms, by combining a computational exploration of their conformational landscapes with an experimental determination of their conformer-specific near-infrared (IR) vibrational spectra. These were obtained through double resonance IR–UV and UV–UV hole burning (HB) and IR ion dip (IRID) spectroscopy,[10] Manα(1,3)Manφ (**1**) and Manα(1,6)Manφ (**2**) with the UV chromophore provided by a phenyl tag, φ (Figure 2).

Materials and Methods

Synthesis and Vaporization. Labeled disaccharides **1** and **2** were accessed from the Lewis acid catalyzed glycosylation between participatory mannosyl trichloroacetimidate glycosyl donors, and regioselectively protected benzylidine-2-*O*-benzyl, or 2,3,4-*O*-triacetyl phenyl mannoside acceptors, respectively. The resulting protected disaccharide intermediates underwent subsequent catalytic hydrogenation and transesterification to give **1** and **2** in excellent yield (see Supporting Information for more details).

Transfer of the dimannosides into the gas phase through evaporation from a high temperature oven was not appropriate because of their facile decomposition, but laser desorption caused only minor fragmentation and was the method of choice. As well as keeping the fragile dimannosides intact in the gas phase, laser desorption was also much more sample conservative than oven evaporation—a valuable advantage for samples, such as **1** and **2**, that can only be synthesized economically in relatively small amounts. The powdered samples were ground with graphite powder (1:10 graphite/disaccharide approximate mass ratio) and deposited as a thin uniform surface layer on a graphite substrate, which was then placed in the vacuum chamber close to the exit of a pulsed, cylindrical nozzle expansion valve (0.8 mm diameter). Molecules desorbed from the surface using the fundamental of a pulsed and focused Nd:YAG laser were entrained and cooled in an expanding argon jet (~4 bar backing pressure) before passing into the detection chamber through a 1 mm diameter skimmer.

Spectroscopy Schemes. The conformational structures of the two dimannosides, **1** and **2**, were explored spectroscopically, using methods that have proved to be very successful in recent investigations of a range of monosaccharides[11–15] and the disaccharide, lactose.[16] Their conformer specific near-IR spectra were recorded through a combination of mass-selected resonant two photon ionization (R2PI), double resonance UV–UV and near-IR–UV hole burning (HB), and near-IR ion dip (IRID) spectroscopy. (The level of resolution of resonant features in the recorded R2PI band spectra also provided a valuable indicator of the efficiency of cooling, following entrainment of the disaccharides in the supersonic expansion.) UV–UV or IR–UV hole burning established the number of distinguishable conformers populated in the expansion, and their individual near-IRID spectra provided the distinctive patterns of OH stretching modes associated with each detected conformer. In the case of **2**, where the R2PI signal was too weak to perform efficient UV–UV HB spectroscopy, the more efficient IR–UV hole burning strategy was used to identify individual conformers after recording their IRID spectra. In this strategy, an IR burn laser is tuned onto a selected vibrational transition identified in the IRID spectrum and associated with a specific conformer (in the ground electronic state); in the UV hole burn scheme, the UV burn laser was tuned onto a selected vibronic transition identified in the R2PI spectrum.

The R2PI detection scheme necessarily relies on the observation of the $S_1 \leftarrow S_0$ electronic transition of an UV chromophore, provided in the present investigation by the phenyl tag attached to one end of the disaccharide (O1). Fortunately, the tag does not alter its low-lying conformational preferences (see later discussion and ref 11). In one sense indeed, it can even be seen as an advantage: the phenyl ring mimics to some extent the neighboring monosaccharide residue in larger oligosaccharides, where one end of the glycosidic linkage is also located at O1.

Computational Exploration of the Conformational Landscapes. A comprehensive investigation of the conformational landscapes of the dimannosides and the identification of their most stable structures presents a major computational effort, given their size and conformational flexibility; the strategy adopted followed a similar sequence to that employed in previous studies of benzyl lactoside,[16] a series of

(10) Robertson, E. G.; Simons, J. P. *Phys. Chem. Chem. Phys.* **2001**, *3*, 1–18.
(11) Çarçabal, P.; Jockusch, R. A.; Hunig, I.; Snoek, L. C.; Kroemer, R. T.; Davis, B. G.; Gamblin, D. P.; Compagnon, I.; Oomens, J.; Simons, J. P. *J. Am. Chem. Soc.* **2005**, *127*, 11414–11425.
(12) Jockusch, R. A.; Talbot, F. O.; Simons, J. P. *Phys. Chem. Chem. Phys.* **2003**, *5*, 1502–1507.
(13) Talbot, F. O.; Simons, J. P. *Phys. Chem. Chem. Phys.* **2002**, *4*, 3562–3565.
(14) Hunig, I.; Painter, A.; Jockusch, R. A.; Çarçabal, P.; Marzluff, E. M.; Snoek, L. C.; Gamblin, D. P.; Davis, B. G.; Simons, J. P. *Phys. Chem. Chem. Phys.* **2005**, *12*, 2474–2480.
(15) Çarçabal, P.; Patsias, T.; Huenig, I.; Liu, B.; Kaposta, E. C.; Snoek, L. C.; Gamblin, D. P.; Davis B. G.; Simons, J. P. *Phys. Chem. Chem. Phys.* **2006**, *8*, 129–136.
(16) Jockusch, R. A. et al. *J. Am. Chem. Soc.,* **2004**, *126*, 5709–5714.

monosaccharides[11-15] and their hydrated complexes.[11,12,14,15] To be as conservative as possible in terms of computational time, however, redundant or irrelevant conformations were screened by gradually increasing the level of theory, and the ONIOM method[17] was used to perform the geometry optimizations and (harmonic) frequency calculations of selected conformations rather than the standard density functional theory used previously.[11-16]

An initial set of conformations was generated by random conformational searches using the Tripos and MMFFs force fields, and the resulting structures were initially optimized at the HF/3-21G level of theory; several different structures converged into the same minimum. After removal of these duplicates, single-point B3LYP/6-31+G(d) and MP2/6-31+G(d) energy calculations were performed to eliminate very high energy conformations before optimizing the remaining structures and calculating their IR spectra at the ONIOM B3LYP/6-31+G(d): HF/3-21G (carbohydrate/phenyl ring) level. The calculated harmonic vibrational frequencies were scaled by a factor of 0.9734 for comparison with the experimental IR spectra, a factor that has proven to be adequate in the earlier carbohydrate investigations.[11-16]

The force field conformational search generated about 150 different conformations for both disaccharides, and a selection of 68 conformers of Manα(1,3)Manφ and 98 conformers of Manα(1,6)Manφ reached the last step of the computational progression. Their relative energies were obtained by MP2/6-31+G(d)//B3LYP/6-31+G(d):HF/3-21G single-point energy calculations, corrected by the zero-point energies derived from the ONIOM B3LYP/6-31+G(d):HF/3-21G frequency calculations.

In the case of the dimannoside **2**, the molecule could fold because of the higher flexibility of the α(1,6) glycosidic linkage, and in several of its low-lying conformers, the phenyl ring could interact with the terminal pyranose ring. Although this interaction will be underestimated in an ONIOM calculation that treats the phenyl tag at the HF level of theory, comparison between the experimental and the calculated spectra of the OH stretching modes (mostly influenced by electrostatic interactions) allowed elimination of these conformers as possible assignments. The ONIOM strategy was retained, therefore, to sustain a balance between a comprehensive conformational search and a sustainable computational cost, and the relative energies and structures of the most stable conformers were computed at the ONIOM MP2/6-311++G(d,p):HF/3-21G(d)//ONIOM B3LYP/6-31+G(d):HF/3-21G-(d) level. All the quantum chemistry calculations were performed using the Gaussian 03 software package.[18]

Results and Conformational Assignment

Manα(1,3)Manφ. The R2PI spectrum of the mannose disaccharide **1**, shown in Figure 3, presents a series of resonant transitions superimposed on a broad, underlying continuum, in marked contrast to the R2PI spectra presented by phenyl tagged monosaccharides.[11-15] This could be due to spectral congestion arising from the superposition of the R2PI spectra of several unresolved conformers or to incomplete cooling in the supersonic expansion, leading to an unresolved contribution from vibrational hot-bands, or perhaps to a higher density of vibronic states. Fortunately, the issue could be resolved through a combination of hole burning and IRID experiments.

The UVHB spectrum, also shown in Figure 3, faithfully reproduced all the resonant features of the R2PI spectrum but not the broad unresolved underlying absorption; all the resonant features share the same ground state and are associated with a unique carrier. When the R2PI spectrum was probed by IRID spectroscopy, regardless of the selected probe laser wavelength,

(17) Maseras, F.; Morokuma, K. *J. Comput. Chem.* **1995**, *16*, 1170−1179. Dappich, S.; Komaromi, I.; Byun, S.; Morokuma, K. J.; Frisch, M. J. *J. Mol. Struct.* **1999**, *451*, 1−21.
(18) Frisch, M. J. et al. *Gaussian 03*, Revision B.03; Gaussian, Inc.: Pittsburgh, PA, 2003.

1: Manα(1,3)Manφ

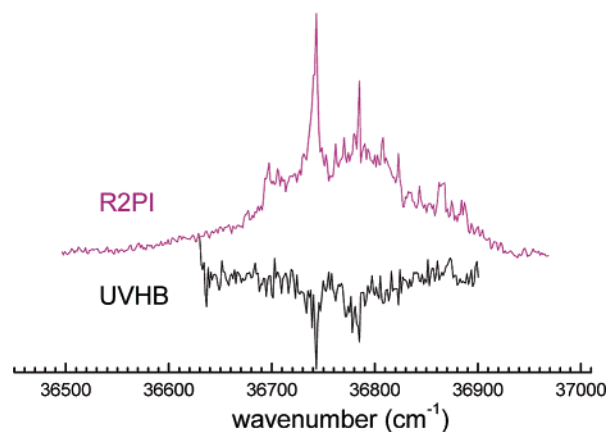**Figure 3.** R2PI (upper) and UVHB (lower) spectra of Manα(1,3)Manφ; the hole burn spectrum was recorded with the burn laser tuned to the most intense resonant feature at 36 743 cm⁻¹. An identical UVHB spectrum was generated when the burn laser was centered on the weaker feature at 36 785 cm⁻¹.
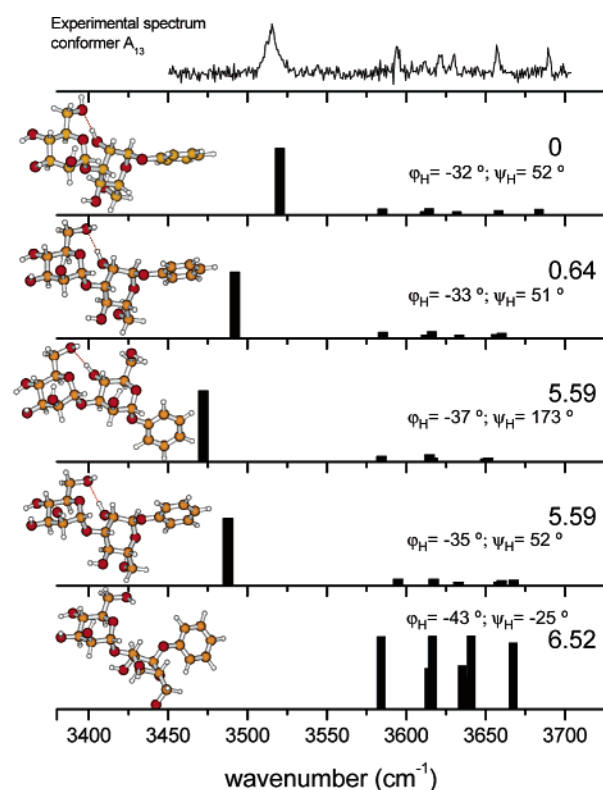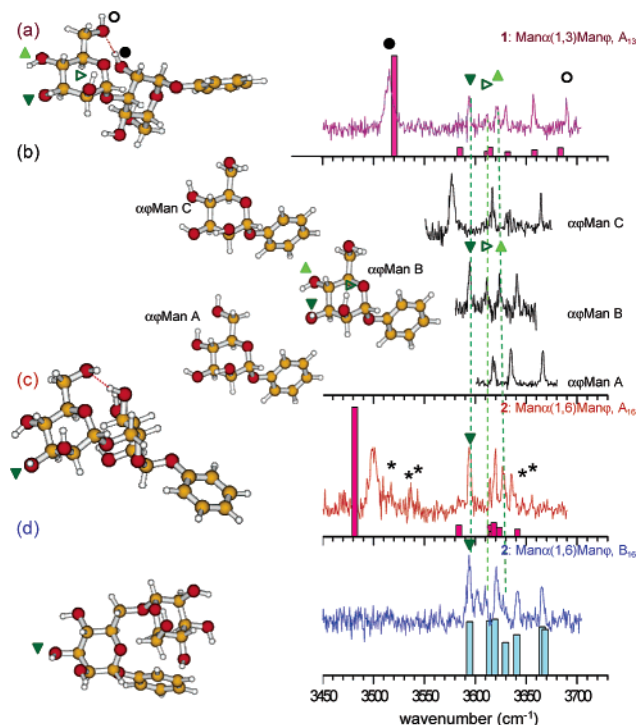

Figure 4. Experimental IRID spectrum of Manα(1,3)Manφ and the computed IR spectra of its five lowest-lying conformers. Relative energies in kJ mol⁻¹; glycosidic dihedral angles defined as $\varphi_H(H1'-C1'-O-C3)$ and $\psi_H(C1'-O-C3-H3)$. Larger scales structures are given in the Supporting Information.

the same vibrational spectrum was always observed: it follows that both the sharp resonant features in the R2PI spectrum and the underlying continuum are associated with the same, unique carrier, which favors assignment of the unresolved background to the excitation of congested hot-band transitions.

The IRID spectrum is presented in Figure 4, together with the IR spectra computed for the five lowest-lying conformers of the disaccharide. The experimental spectrum includes seven distinct bands, corresponding exactly to the number expected from one single conformer given the number of OH groups in

Figure 5. (a, c, and d) Infrared ion dip (IRID) spectra, structures, and predicted spectra of the calculated conformation to which the observed species are assigned. (b) IRID spectra of the observed conformers of the monosaccharide, $\alpha\varphi$Man;[11] the dotted lines link corresponding OH vibrational bands in the disaccharides to those in conformer B of the monosaccharide. The symbols connect the observed band to the OH group to which they are assigned. The asterisks in panel d suggest the contamination of the spectrum of A_{16} by other minor conformers.

Figure 6. R2PI (upper) and IRHB (middle and lower) spectra of Manα-(1,6) Manφ. The arrows indicate the features of the R2PI spectrum probed for IRID measurements.

the disaccharide. It is in close correspondence with the spectrum associated with the global minimum energy conformation, and it presents no additional features (spectral contamination) that could indicate the presence of other conformers. If they were present and if the underlying continuum were associated with their overlapping band systems, additional features would be anticipated. In summary, the indication is clear; only one conformer of Manα(1,3)Manφ (labeled A_{13}) is significantly populated in the cold supersonic expansion.

Figure 5 compares the near-IRID spectrum of the disaccharide conformer A_{13}, with the corresponding spectra of the three populated conformers of the phenyl tagged monosaccharide unit, $\alpha\varphi$Man.[11] It shows two striking differences: a strong and broad absorption band (identified by a full circle) appears in the spectrum of the disaccharide at low wavenumber, $\sim$3515 cm^{-1}, indicating a relatively strong OH $\rightarrow$ O hydrogen bond, and a rather weak and narrow absorption band (identified by an empty circle), typical of a free OH group, appears at a characteristically high wavenumber ($\sim$3690 cm^{-1}). In the β(1,4) linked disaccharide, benzyl lactoside, which incorporates two very strong inter-ring hydrogen bonds, the lowest OH stretching mode is located at $\sim$3400 cm^{-1}.[16] The spectrum associated with the most stable calculated conformer was the only one to reproduce faithfully each of these bands, as well as the five other bands lying between 3590 and 3670 cm^{-1}, and it can be assigned with some confidence to the calculated global minimum structure, shown in Figure 4. The band at a low wavenumber, $\sim$3515 cm^{-1}, is associated with the stretching mode, σ2, of the OH2 group, which is involved in the inter-ring hydrogen bond, OH2
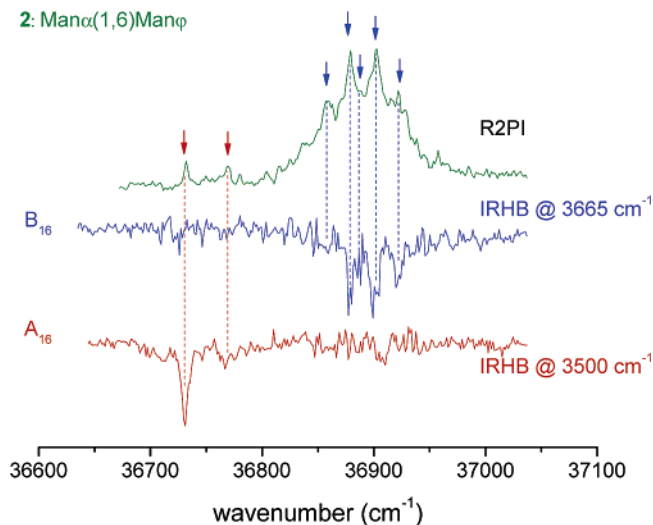
$\rightarrow$ O6$'$, bridging across the glycosidic linkage. The band at a high wavenumber, $\sim$3690 cm^{-1}, corresponds to the mode, σ6$'$, associated with the hydrogen bond acceptor, OH6$'$.

The intermediate IR bands, marked by wedges in Figure 5a, provide further support for this assignment. They are associated with the stretching modes σ3$'$, σ2$'$, and σ4$'$ of the three OH groups (also indicated by wedges on the accompanying structure) in the disaccharide and are engaged in the same intra-ring hydrogen bonded network as the corresponding OH groups in conformer B of the monosaccharide, $\alpha\varphi$Man (see Figure 5b): their wavenumbers and their relative intensities are in near perfect correspondence with those of the disaccharide. The displacement of the fourth band, σ6$'$, to high wavenumbers relative to its position in the monosaccharide reflects a stiffening of the O$-$H bond, induced by its role as an acceptor in the inter-ring hydrogen bond, OH2 $\rightarrow$ OH6$'$.

Manα(1,6)Manφ. The R2PI spectrum of the α(1,6) linked dimannoside shown in Figure 6 differs markedly from the corresponding spectrum of the α(1,3) disaccharide. It is spread over a wider spectral range and presents two distinct components: a weak band system at low wavenumbers and a stronger one at higher wavenumbers. Under similar source conditions, the R2PI signals for Manα(1,6)Manφ were about half those for Manα(1,3)Manφ, a first indication of signal dilution over more than one conformer. Their intensities were too poor, unfortunately, to allow reliable UVHB measurements, but reproducible IRID spectra could be recorded.

A series of measurements probing each of the two regions of the R2PI spectrum generated the two IRID spectra shown in Figure 5c,d, associated respectively, with R2PI probe transitions located on the low and high wavenumber systems and identified by the sets of red and blue arrows in Figure 6. The two distinct spectral signatures imply the population of (at least) two conformers in the free jet environment; they are labeled A_{16} and B_{16}. One of them, A_{16}, displays a strongly displaced and broadened vibrational band at $\sim$3500 cm^{-1}, cf. the conformer A_{13} of the α(1,3) disaccharide, but the other does not.

When IR$-$UV hole burn experiments were conducted with the burn IR laser tuned to the absorption band located at 3500 cm^{-1} (A_{16}) and 3665 cm^{-1} (B_{16}), they generated the two
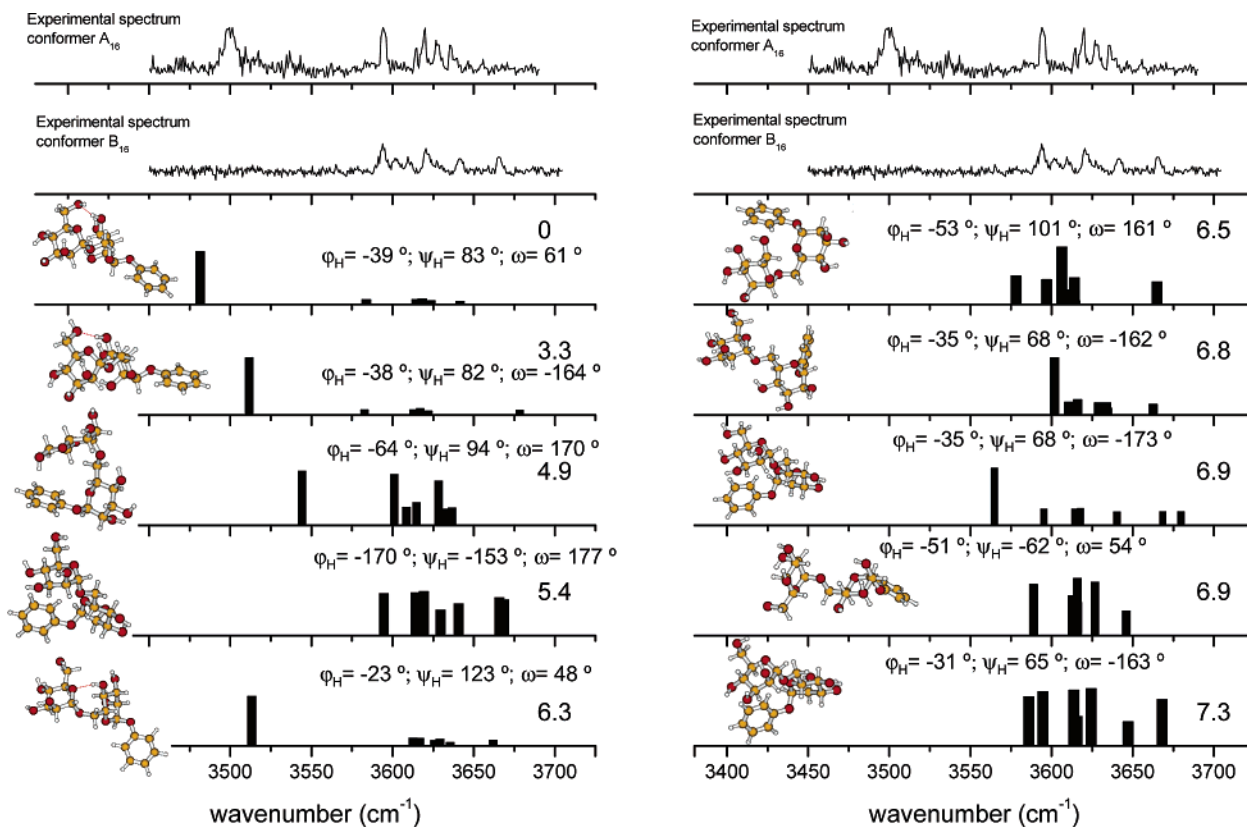
Figure 7. Experimental IRID spectrum of Manα(1,6)Manφ and the computed IR spectra of its 10 lowest-lying conformers. Relative energies in kJ mol^{-1}; glycosidic dihedral angles defined as φ_H(H1′−C1′−O−C6), ψ_H(C1′−O−C6−H6), and ω(O−C6−C5−C4). The structures can be seen on a larger scale in the Supporting Information.

characteristic HB spectra shown in the lower half of Figure 6. The HB spectra faithfully reproduced each of the corresponding resonant band systems displayed in the R2PI spectrum (but not the underlying continuum), confirming their association with the two distinct conformers, A_{16} and B_{16}; their relative R2PI spectral intensities suggest that B_{16} is the more favored. The IRID spectrum associated with the B_{16} region of the R2PI spectrum displays seven distinct bands, which correspond to the number expected from a single conformer. The sharp resonant features in the R2PI spectrum and the underlying continuum must be associated with the same carrier, and the unresolved background, as with the α(1,3) disaccharide, must be associated with the excitation of its congested hot-band transitions. The IRID spectrum associated with excitation in the region of conformer A_{16}, shown in Figure 5c, which exhibits a strongly shifted and broadened band at ∼3500 cm^{-1}, closely resembles the IRID signature of the α(1,3) disaccharide, again indicating a conformational structure stabilized by a single inter-ring hydrogen bond. In contrast to both A_{16} and A_{13}, however, none of the bands associated with the other conformer, B_{16}, is strongly displaced in the IRID spectrum: like the free αφMan monosaccharide conformers A, B, and C, they all occupy the same spectral region, and there is no inter-ring hydrogen bonding.

The α(1,6) linkage involves the exocyclic hydroxymethyl group of one of the monosaccharide subunits. The extra bond in the linkage reduces steric interactions between the subunits and enhances their relative conformational flexibility[9] to create a wide range of potentially accessible low energy conformations. Their predicted structures and near-IR spectra fall into two

distinct categories: those that display a (single) inter-ring hydrogen bond signaled by a strongly shifted and intensified OH band located in the range of ∼3500−3550 cm^{-1} and those that do not (see Figure 7).

The calculated IR spectra associated with (at least) two of the low energy structures selected from the conformations shown in Figure 7 reproduce the main features of one or other of the experimental IRID spectra quite well. One of them corresponds with the calculated global minimum energy structure, and it is shown again in Figure 5c. It presents an inter-ring hydrogen bond, OH4 → O6′, that stiffens the glycosidic linkage, and its predicted IR spectrum provides a close match with that of conformer A_{16}. Additional weaker absorption bands in the IRID spectrum of A_{16}, identified by asterisks in Figure 5c, also suggest the population of other minor conformers with UV absorption bands overlapping those associated with A_{16}. The appearance of additional weak features located between 3500 and 3550 cm^{-1} would be consistent with the population of other (minor) conformers that also incorporate inter-ring H bonding and are calculated to lie at energies intermediate between the global minimum structure, assigned to A_{16}, and the lowest energy structure that lacks an inter-ring hydrogen bond, located at a calculated relative energy of 5.4 kJ mol^{-1} (see Figure 7). Its calculated IR spectrum is quite similar to the experimental IRID spectrum associated with conformer B_{16}, encouraging its tentative assignment to the corresponding structure, shown in Figure 5d.

Although the structure assigned to conformer A_{16} corresponds to the calculated global minimum, the R2PI spectrum associated with B_{16} is much more intense. This could be explained if the

entropy gain associated with its higher flexibility favors its population at the initial elevated temperature of the vaporization source and the structure is frozen in the early stages of the free jet expansion. Relaxation into the global potential energy minimum would be inhibited if the barrier to conversion from B_{16} to A_{16} was much higher than the energy of the collisions experienced in the expansion. The opposite situation was met in benzyl lactoside[16] where the minimum potential energy structure, a rigid conformer with two strong inter-ring H bonds, was stabilized in the free jet expansion, although free energy calculations suggested that it was not favored at high temperatures.

In contrast to the α(1,3) disaccharide, comparisons between the IR spectra of the two principal conformers A_{16} and B_{16} and those of its constituent monosaccharide units do not suggest clear correspondences. Each of the suggested conformational assignments includes a mannose subunit in which the OH groups are arranged in a counterclockwise arrangement, as in αφMan B, and a comparison of the calculated and experimental IR spectra associated with A_{16} and B_{16} does indicate a clear connection between the vibrational bands observed at 3694 cm^{-1} (indicated by a wedge in Figure 5c,d) and the corresponding band in the IR spectrum of αφMan B: both are associated with the $\sigma3'$ stretching mode. A correspondence with the other bands of the spectrum of conformer B of αφMan is also suggested (indicated by the dotted lines in Figure 5), but the congested IRID spectra and the uncertainties in their detailed assignments, particularly of the conformer B_{16}, make comparisons difficult.

Conclusion

Despite the challenge in tackling such a complicated conformational landscape, there is good reason to be confident about the coarse-grained structural assignments, based upon the qualitative analysis of the observed spectral signatures, the match between the observed and calculated spectra associated with the low-lying conformers, their relative energies, and where possible, comparisons between the spectra of the disaccharide conformers and their monosaccharide components. Conformational assignments as definite and precise as those that can be obtained for smaller molecules are beyond the scope of current strategies, but there is no doubt about the distinction between the two conformational families now identified: those with, A_{13} and A_{16}, or without, B_{16}, a (single) inter-ring hydrogen bond. The ability to separate and assign such structures experimentally will help in identifying the regions of larger oligosaccharides that can provide some rigidity, or a source of flexibility, or targets for the binding of structural water molecules.[11]

The general IR spectral signatures that have been characterized, as well as identifying membership of broad conformer families, can also identify noninteracting, free OH groups that are potentially important sites for interaction with the environment.[9,11] The spectrum of conformer A_{13} in Manα(1,3)Manφ provides an excellent example. There is an inter-ring hydrogen bond, linking OH2 to O6′, which shifts the IR absorption of its stretching mode to 3520 cm^{-1}, but OH6′ does not interact with any other group in the molecule—which makes it an ideal binding site for solvent molecules[11]—and the associated stretch-

ing band absorbs at a high wavenumber, 3690 cm^{-1}. In larger oligosaccharides, more severe IR spectral congestion can be anticipated, but it will be concentrated mainly in the intermediate spectral region lying between 3600 and 3650 cm^{-1}, where intraring H bonded OH groups absorb. The high and low wavenumber ends of the spectrum should remain much clearer and continue to provide reliable indicators of the conformational families to which the conformers belong.

The spectral features of the isolated monosaccharide residues may also be used to refine the assignment of larger oligosaccharide structures. This provides a more general supplementary building block approach to the study of complex structures, based upon an alphabet of established IR spectral signatures of different conformations of the monosaccharide unit—when their spectroscopic patterns are retained. If they are not retained, their evolution can be understood by analyzing the modification of the hydrogen bonded networks in the disaccharides, for example, the retention (or disruption) of the secondary structural motifs generated by intraresidue H-bonding. The concept of secondary structure for carbohydrates has not been addressed very clearly yet. The spectral analysis of their IR spectra can be eased by considering each monosaccharide unit in a larger carbohydrate structure, as a module with or without interactions promoted by inter-ring H bonds.

Finally, feedback from the increasing body of experimental data will help to inform and guide future theoretical conformational searches. It is possible that using IR spectra of subunits of a large system to understand its own vibrational spectroscopy and guide the fine-tuning of the computational conformational identification will meet some limitations due to spectral congestion as the size of the system increases, but the computational time bottleneck will probably occur much earlier. If the conformational search can be informed by experiment to include only those geometries that incorporate features clearly identified by the experimental spectrum, it should be possible to extend further the limits of the current strategy. This will prove essential for defining the intrinsic conformational preferences of larger oligosaccharides going toward the core pentasaccharide of N-linked glycans.

Supporting Information Available: Detailed description of the synthesis and characterization of **1** and **2**. Cartesian coordinates and total energies of the conformations assigned to A_{13}, A_{16}, and B_{16}. Complete refs 16 and 18. Larger scale display of the conformations of **1** and **2** shown in Figures 4 and 7. This material is available free of charge via the Internet at http://pubs.acs.org.

JA055891V